Electronic Supplementary Material (ESI) for Nanoscale Advances.
This journal is © The Royal Society of Chemistry 2025

Electronic Supplementary Material

Magnetic Hyperthermia Triggered Multi-Functional Thermo-Responsive Lipid Nanoparticles for Enhanced Paclitaxel Release and Cytotoxicity

Preparation of γ-Fe_2O_3 loaded TLN

PTX is soluble in ethanol, acetonitrile, and methanol (50 mg/cm^3) [1]. Alternatively, it has low water solubility [2], and high hydrolytic potential when exposed to different aqueous and organic media. It is rapidly destroyed in weakly alkaline [3] and strongly acidic aqueous solutions, whereas the lowest amount of degradation in aqueous solutions occurs at weakly acidic pH (3 to 5) [4]. PTX solution of methanol undergoes hydrolysis and transesterification of ~30% after two weeks of storage at room temperature. Surfactant action on hydrophobic PTX employing Cremophor EL and ethanol blend (1:1) diluted with 5–20 fold (30 mg paclitaxel dissolved in 5 mL-paclitaxel; Bristol-Myers Squibb) in aqueous solution [5] solubilizes and inhibits hydrolysis. CrEL is FDA approved, and already clinically used for intravenous injection [6]. Cremophor EL is a thermally stable and hydrophilic [7] non-ionic polyoxyethylated surfactant [8] with an HLB value of 13.5 [9]. During the emulsification process, high temperature may destabilize the TLN and change the curvature of the surfactant structure, which is prevented by the incorporation of highly thermally stable Cremophor EL [10].

The structure of the nanoparticle shell has a significant impact on physicochemical properties, drug release or leakage [11]. The leakage of payload is faster in the case of nanoparticles with large pores [12] which are covered by a layer of larger surfactant molecules [13].

Solid saturated fatty acid based lauric acid is responsible for drug release upon degradation at neutral pH. Lauric acid is insoluble in water, but laurate has a solubility of more than 1000 µM in the buffer of pH 7.4 [14]. Conversion of insoluble lauric acid to laurate depends on the pH of the medium i.e., no dissociation at pH < 4, while laurate ions are generated at circum-neutral pH and pH > 9 all lauric acid is in the form of laurate ions [15].

Factorial Optimization

Design of Experiments (DOE) is a method used to analyze the responses by exposing them to a set of different variables involving the least number of experiments runs to obtain the maximum optimum conditions.

Table S1: Best-fit model validation by examining ANOVA, F-value, lack of fit P-value, R^2, adjusted-R^2 - predicted-R^2, coefficient of variance (%CV), and adequate precision (ADP).

Parameter	**Model**	***P*-value**	**Lack of Fit *P*-value**	***F*-value**	**R^2**	**Adjusted R^2 - Predicted R^2**	**ADP**	**%C.V.**	
Particle size	Linear	< 0.0001	0.1809	14.02	0.7244	0.1449	11.2427	15.24	Suggested
Polydispersity	Linear	0.0038	0.2779	6.74	0.5584	0.2227	8.7747	15.24	Suggested
Zeta potential	Linear	< 0.0001	0.5846	37.65	0.8759	0.0346	20.1769	6.82	Suggested
EE of PTX	2FI	0.0526	0.0823	3.71	0.9668	0.0995	30.1397	5.31	Suggested
EE of γ-Fe_2O_3	2FI	0.0228	0.5767	4.48	0.9236	0.065	18.3324	5.48	Suggested

Table S2: ANOVA results obtained from design expert analysis to validate the accuracy of all the experimental coefficients.

Source	A-Surfactant/Co-Surfactant	P-γ-Fe2O3	C-Stirring Speed	AB	BC	AC
Particle size	0.0004	0.0002	0.9018	-	-	-
Polydispersity	0.0207	0.2525	0.003	-	-	-
Zeta potential	< 0.0001	0.0073	0.0359	-	-	-
EE of PTX	< 0.0001	< 0.0001	< 0.0001	0.0453	0.2137	0.0872
EE of Fe_2O_3	< 0.0001	< 0.0001	0.0015	0.0034	0.7025	0.5016

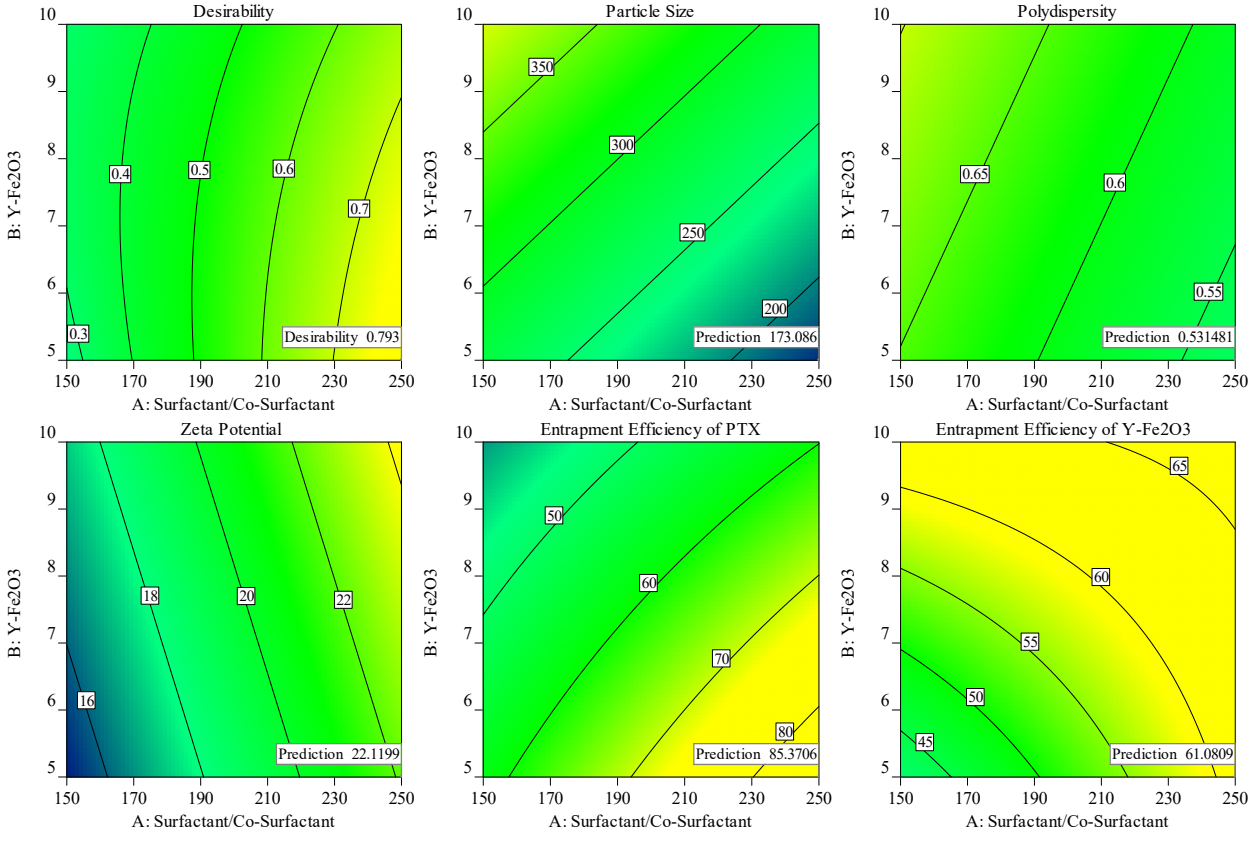

Figure S1: Contour illustration of desirability and interaction factor AB, for all the dependent variables.

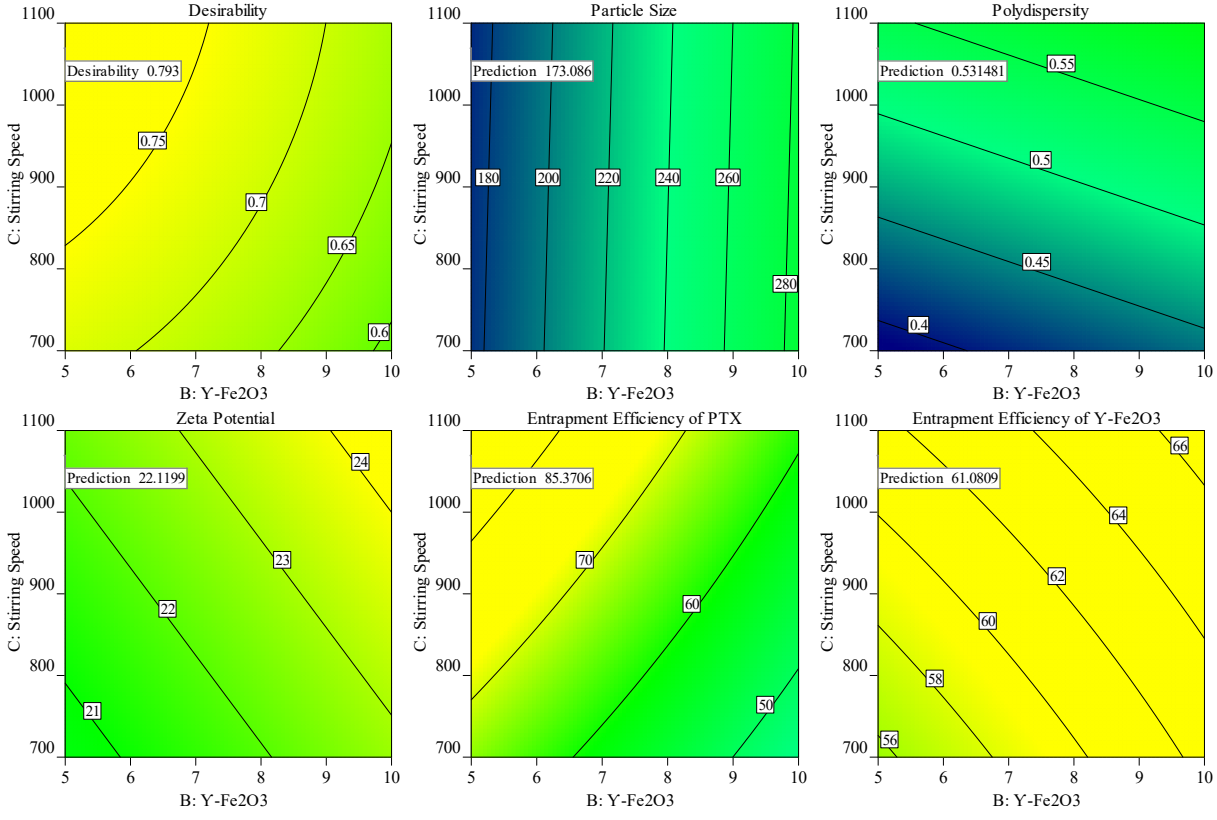

Figure S2: Contour illustration of desirability and interaction factor BC, for all the dependent variables.

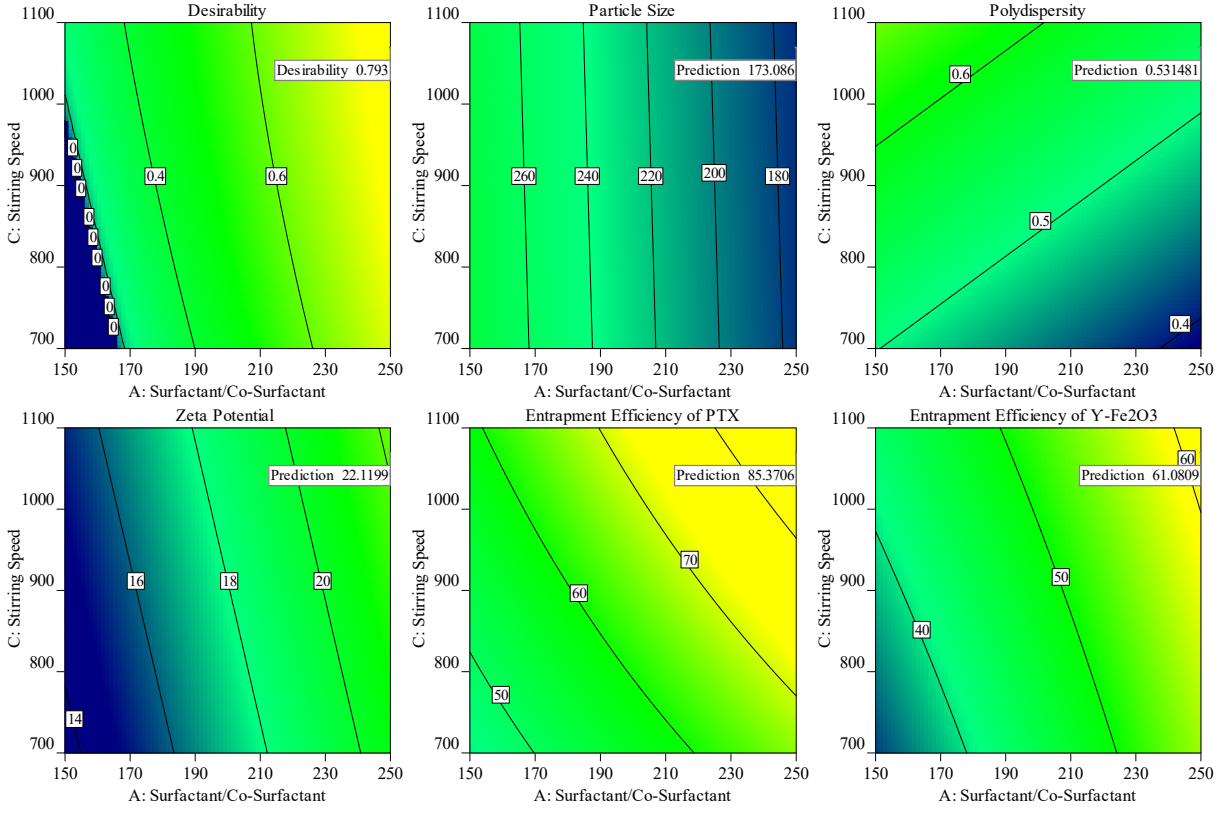

Figure S3: Contour illustration of desirability and interaction factor AC, for all the dependent variables.

Characterizations:

Determinization of hydrodynamic diameter PDI and zeta potential:

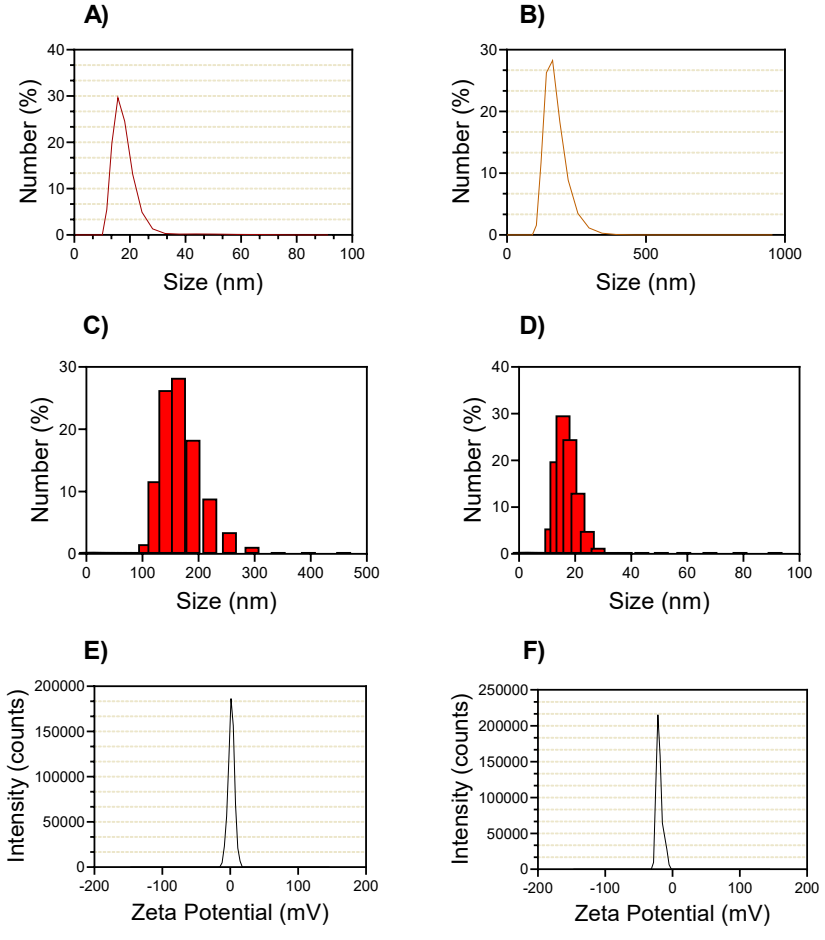

Figure S4: Size measurements for γ-Fe_2O_3 and P-γ-TLN (A and B), size distribution analysis (C and D), and zeta potential measurements (E and F)

Compatibility analysis and Solid-State characterization:

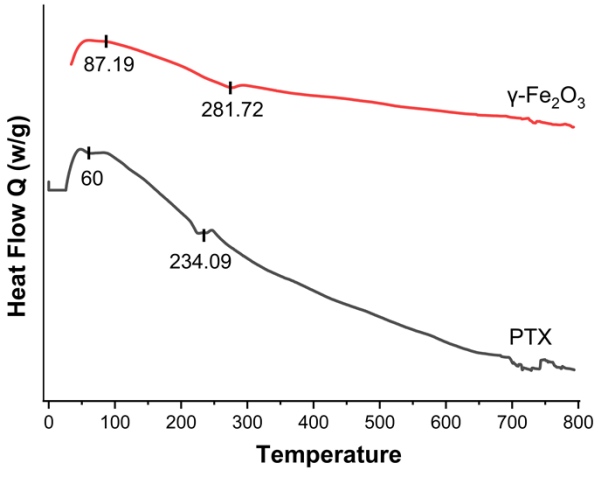

Figure S5: Thermograms for pure PTX and γ-Fe_2O_3 depicting degradations and melting.

Table S3: Calorimetric data depicting temperature variation, thermal stability, and thermal transitions in ingredients and lipid formulations.

Material	Onset (°C)	Melting peak (°C)	Endset (°C)	Δ*H* Melting enthalpy J/g	Tm-To
Lauric Acid	45.40	48.08	76.12	72.478	2.68
PTX	25.42	234.09	647.84	505.16	-
γ-Fe_2O_3	34.15	275.88	712.2	1129.7	-
P-γ-TLN (10 mg)	23.23	39.52	47.51	7.1695	16.29
P-γ-TLN (15 mg)	42.35	52.96	63.26	306.58	10.61

***In vitro* magnetic evaluations:**

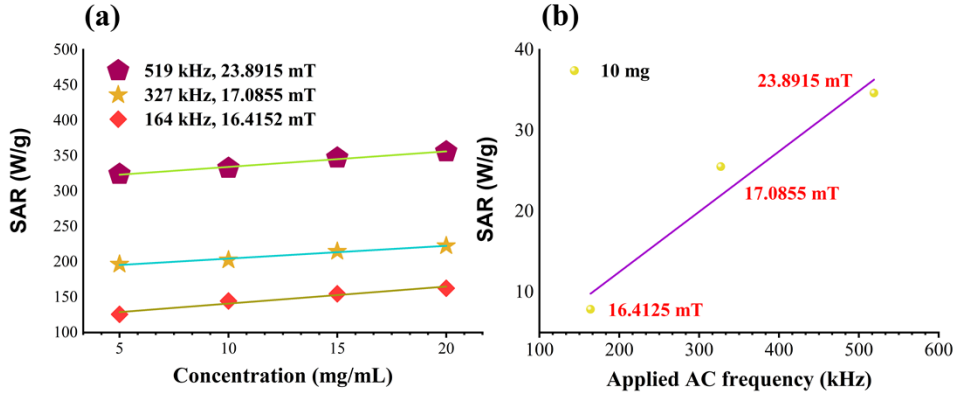

Figure S6: *SLP* of γ-Fe_2O_3 fluid samples measured in an ac magnetic field of different fields and frequencies as a function of concentration and (b) *SLP* of γ-Fe_2O_3 encapsulated TLN lyophilized samples measured at different fields and frequencies. The straight lines are a guide to the eye.

In vitro drug release study**:**

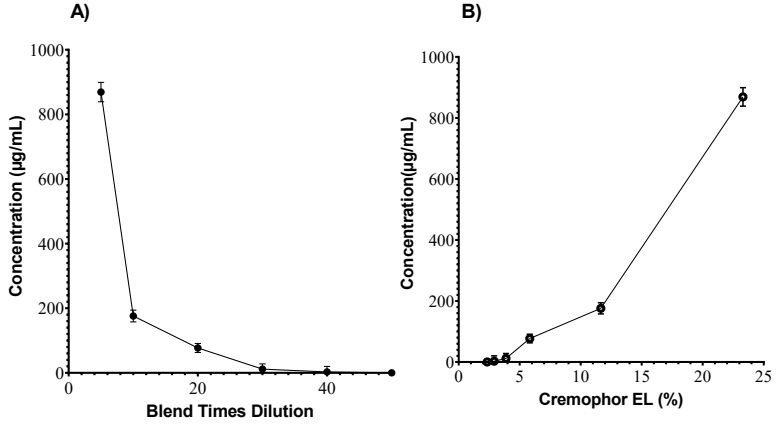

Figure S7: Dissolution estimation using Cremophor EL blend in terms of blend times (A) and percentage (B) corresponding to the PTX concentration (µg/mL).

Stability studies:

Table S4: Stability parameters for optimized P-γ-TLN 12 following phase IVa for a period of twelve months.

Type of study	Parameters	Months						Change%
		0	1	3	6	9	12	
Long-term 5°C ± 3°C	Particle size	183.1	182.7	183.9	187.7	193.1	192.7	5.17
	PDI	0.507	0.517	0.522	0.547	0.527	0.585	3.79
	Entrapment of PTX	85.37	83.23	83.35	82.32	80.39	80.47	5.73
	Entrapment of γ-Fe_2O_3	60.49	60.21	58.24	56.11	56.21	56.17	7.69
Accelerated 25°C ± 2°C	Particle size	183.1	182.1	188.2	191.6	-	-	4.43
	PDI	0.507	0.526	0.522	0.536	-	-	13.92
	Entrapment of PTX	85.37	84.23	81.39	81.03	-	-	5.08
	Entrapment of γ-Fe_2O_3	60.49	60.02	57.21	54.29	-	-	11.82

References:

[1] Vyas, D. M.; & Kadow J. F. Paclitaxel: a unique tubulin interacting anticancer agent. *Prog. Med. Chem.* **1995**, 32, 289-337.

[2] Ma P.; & Mumper R. J. Paclitaxel nano-delivery systems: a comprehensive review. *J. Nanomed. Nanotech.* **2013**, 4, 1000164.

[3] Richheimer S. L.; Tinnermeier D. M.; & Timmons D. W. High-performance liquid chromatographic assay of taxol. *Anal. Chem.* **1992**, 64, 2323-2326.

[4] Xu Q.; Trissel L. A.; & Martinez J. F. Stability of paclitaxel in 5% dextrose injection or 0.9% sodium chloride injection at 4 22 or 32° C. *Am. J. Health-Syst. Pharm.* **1994**, 51, 3058-3060.

[5] Gelderblom H.; Verweij J.; Nooter K. & Sparreboom A. Cremophor EL: the drawbacks and advantages of vehicle selection for drug formulation. *Eur. J. Cancer.* **2001,** 37, 1590-1598.

[6] Chen Y.; Yang X.; Zhao L.; Almásy L.; Garamus V. M.; Willumeit R.; & Zou A. Preparation and characterization of a nanostructured lipid carrier for a poorly soluble drug. *Coll. Surf A: Physicochem. Eng. Asp.* **2014**, 455 36-43.

[7] Adel S.; Fahmy R. H.; Elsayed I.; Mohamed M. I.; & Ibrahim R. R. Exploiting itraconazole-loaded nanomixed micelles in coated capsules as efficient colon-targeted delivery system for improved antifungal and potential anticancer efficacy. *Pharm. Dev. Tech.* **2023**, 28, 333-350.

[8] Chiang J.-L.; & Yang Y.-W. Modulation of the anticancer activities of paclitaxel by Cremophor micelles. *International J. Pharm.* **2021**, 603, 120699.

[9] Shakeel F. Criterion for excipients screening in the development of nanoemulsion formulation of three anti-inflammatory drugs. *Pharm. Dev. Tech.* **2010**, 15, 131-138.

[10] Kaur P.; Mishra V.; Shunmugaperumal T.; Goyal A. K.; Ghosh G.; & Rath G. Inhalable spray dried lipidnanoparticles for the co-delivery of paclitaxel and doxorubicin in lung cancer. *J. Drug Del. Sci. Tech.* **2020**, 56, 101502.

[11] Huang Z. R.; Hua S. C.; Yang Y. L.; & Fang J. Y. Development and evaluation of lipid nanoparticles for camptothecin delivery: a comparison of solid lipid nanoparticles nanostructured lipid carriers and lipid emulsion. *Acta. Pharmacol. Sin.* **2008,** 29, 1094-1102.

[12] Gao Y.; Chen Y.; Ji X.; He X.; Yin Q.; Zhang Z.; Shi J.; & Li Y. Controlled intracellular release of doxorubicin in multidrug-resistant cancer cells by tuning the shell-pore sizes of mesoporous silica nanoparticles. *ACS Nano.* **2011**, 5, 9788-9798.

[13] Souto E.; Almeida A.; & Müller R. Lipid nanoparticles (SLN® NLC®) for cutaneous drug delivery: structure protection and skin effects. *J. Biomed. Nanotech.* **2007**, 3, 317-331.

[14] Vorum H.; Brodersen R.; Kragh-Hansen U.; & Pedersen A. O. Solubility of long-chain fatty acids in phosphate buffer at pH 7.4. *Biochim Biophys. Acta (BBA)-Lipids Lipid Metab*. **1992**, 1126, 135-142.

[15] Earnden L.; Marangoni A. G.; Laredo T.; Stobbs J.; Marshall T.; & Pensini E. Decontamination of water co-polluted by copper toluene and tetrahydrofuran using lauric acid. *Sci. Rep.* **2022**, 12, 15832.